International Journal of Nanomedicine

Dovepress
open access to scientific and medical research

Open Access Full Text Article

ORIGINAL RESEARCH

Three-in-One Nanozyme for Radiosensitization of Bladder Cancer

Yang Li[1], Yuhan Zhang[1], Na Feng[2], Fan Yu[1], Bin Liu[3]

[1]Department of Gastroenterology and Hepatology, China-Japan Union Hospital of Jilin University, Changchun, 130033, People's Republic of China; [2]Department of Laboratory Medicine, Nanfang Hospital, Southern Medical University, Guangzhou, 510515, People's Republic of China; [3]Department of Urology, China-Japan Union Hospital of Jilin University, Changchun, 130033, People's Republic of China

Correspondence: Fan Yu; Bin Liu, Email yufan2017@jlu.edu.cn; liub18@mails.jlu.edu.cn

Purpose: Bladder cancer is a common malignancy of the urinary system and the development of noninvasive therapeutic methods is imperative to avoid radical cystectomy, which results in a poor quality of life for patients.

Methods: In this study, ultrasmall copper–palladium nanozymes decorated with cysteamine (CPC) nanoparticles (NPs) were synthesized to enhance the efficacy of radiotherapy (RT) in treating bladder cancer. CPC NPs react with intracellular overexpressed H_2O_2 in the tumor microenvironment to produce large quantities of reactive oxygen species (ROS) and induce tumor cell apoptosis. Furthermore, the CPC nanozymes can generate ample oxygen within tumors by utilizing H_2O_2, addressing hypoxia conditions, and mitigating radioresistance. Additionally, CPC facilitates the oxidation of glutathione (GSH) into oxidized glutathione disulfide (GSSG), blocking the self-repair mechanisms of tumor cells post-treatment. Simultaneously, CPC enhances the ionization energy deposition effect on tumor cells.

Results: The results demonstrate an increased level of ROS and an elevation in oxygen content at the tumor site. Importantly, tumor growth was restrained without apparent systemic toxicity during the combined treatment.

Conclusion: In summary, this study highlights the potential of CPC nanozyme-mediated radiotherapy as a promising avenue for the effective treatment of bladder cancer and demonstrates its potential for future clinical applications in the synergistic therapy of bladder cancer.

Keywords: bladder cancer, radiotherapy, nanozyme, tumor microenvironment, hypoxia

Introduction

The bladder, a muscular organ responsible for urine storage, is susceptible to carcinogenic factors such as smoking and chemical exposure, leading to the annual diagnosis of over 75,000 cases of bladder cancer.[1–3] This malignancy is among the top 10 causes of cancer-related mortality and typically manifests with symptoms such as hematuria, dysuria, and urinary obstruction.[4–6] The predominant treatment approach involves radical cystectomy, often supplemented by adjuvant chemotherapy.[7–10] In cases where surgical intervention is not optimal, alternative modalities, such as bladder-preserving chemoradiotherapy which drugs and ionizing irradiation are applied, are considered for therapeutic management.[11] Nonetheless, the prolonged application of these clinical therapeutic regimens poses the risk of adverse effects or potential disease recurrence, attributed to incomplete treatment or insufficient self-repair mechanisms in cancer cells.[12] Therefore, to overcome the constraints associated with traditional approaches to bladder cancer treatment and enhance the overall quality of life for patients, there is an urgent need for innovative therapeutic strategies. Specifically, novel approaches within the realm of nanotechnology hold promise for addressing the challenges associated with bladder cancer treatment.[13,14]

Tumor microenvironment (TME) is characterized by mild acidity, hypoxia, overexpressed H_2O_2, and glutathione (GSH).[15–17] This distinct microenvironment develops as a result of the rapid proliferation and heightened metabolism of tumor cells, setting them apart from normal tissues.[18] The hypoxic conditions hinder therapeutic efficacy, while the over-expression of H_2O_2 and GSH potentially diminishes the production of reactive oxygen species (ROS).[19] Consequently, the TME tends to exhibit resistance to therapy, leading to inadequate cancer cell elimination.[20] Addressing this resistance and enhancing therapeutic outcomes necessitates interventions to modulate the TME. Employing an endogenous oxygen

Received: 6 February 2024
Accepted: 3 July 2024
Published: 26 October 2024

generation strategy and augmenting ROS production within tumors become crucial for overcoming these challenges. Catalytical therapy, involving the utilization of enzymes with catalytic properties to modulate the TME, emerges as an innovative and effective antitumor strategy.[21,22]

Catalytic therapy which take the advantage of TME to modulate the chemoresistant or radioresistant status adopt enzymes to obtain desired treatment outcome.Natural enzymes such as glucose oxidase have already been used for starvation therapy for tumors.[23] Catalase (CAT), which generates ROS from H_2O_2, was also applied to enhance tumor inhibition by inducing cell apoptosis. However, these natural enzymes are fragile and only function optimally under specific temperatures and pH values. Their artificial counterparts, nanozymes are capable of functioning under a wide range of extreme environmental conditions and demonstrate a sufficiently high stability.[24,25] Meanwhile, the synthesis of nanozymes is easy to replicate at a relatively low cost. Additionally, their catalytic activities are flexible which can be designed specifically for disease treatment. Among nanozymes, those with peroxidase (POD)-like properties are reported to possess the ability to decompose H_2O_2 into toxic hydroxyl radicals (·OH), which might lead to cell apoptosis. Therefore, POD-like nanozymes have manifested promising potential in ROS-initiated tumor therapy.[26] Some nanozymes with CAT activity can alleviate TME hypoxia by converting H_2O_2 into O_2. More importantly, compared with monometallic nanozymes, bimetallic and trimetallic nanozymes exhibited higher catalytic efficiency.[27–29] For nanozymes with dual enzyme mimicking properties including POD and CAT-like properties, toxic ·OH and O_2 are generated from intracellular H_2O_2 continuously, which improves the radioresistance in tumors. However, the rational design of a nanozyme with a facile synthesis method and multiple enzyme-like properties with high catalytic efficiency in TME was urgent.

Recently, copper-based nanoplatforms have attracted attention in cancer theranostics due to their special properties. These novel nanoplatforms based on copper could be applied to various therapeutic methods, including sonodynamic therapy (SDT), photothermal therapy (PTT), photodynamic therapy (PDT), radiotherapy (RT), and chemodynamic therapy (CDT). Specifically, Cu-doped polypyrrole was developed to amplify the oxidative stress in tumor cells causing severe damage.[30] A cuprous sulfide-based Fe_3O_4@CuS nanoplatform, capable of converting light energy to heat for PTT, was synthesized with specific tumor targeting and deeper tumor penetration characteristics.[31] Core–shell-structured Au@CuS nanoparticles were constructed to induce HeLa cell apoptosis by improved PTT.[32] Cu-based MOF was also applied to enhance the efficacy of radioimmunotherapy.[33] A nanostructure based on disulfiram–copper ion chelation was designed for combinatorial chemotherapy, responding to cues from the TME.[34] An integrated nanoplatform incorporating CuS@Carbon and chlorin e6 demonstrated significant potential for synergistic PTT and PDT. Copper decorated cysteamine (Cys) nanoparticles were synthesized to improve PDT through X-ray irradiation, thereby enhancing the penetration depth of PDT to address both superficial and deep-seated cancers.[35] Concurrently, copper peroxide nanodots, designed to consume overexpressed H_2O_2 in specific TME, demonstrated the capability to generate significant quantities of •OH, inducing tumor cell death.[36] Moreover, copper based nanozyme showed potential in cancer treatment due to POD-like property. Wang et al reported a single atom nanozyme with excellent POD-like activity for multimodal tumor therapy.[37] An nanocomplex consisting of iron atoms and copper atoms with POD-mimicking property was applied for antibacterial applications.[38] Palladium as an important catalyst has been widely utilized for improving the catalytic capacity of nanocomposite. Zhang et al developed single atom Pd/CeO_2 which exhibits high POD and CAT-mimicking activity.[39] Meanwhile, a novel palladium nanozymes with high POD and CAT activity exhibits potential in reprogram macrophages to enhance therapeutic efficacy against colorectal cancer.[40] Given the growing interest in POD and CAT activity of copper and palladium, a facile method was employed to develop ultrasmall Cys-decorated copper–palladium nanoparticles (CPC NPs). This strategy was implemented to treat bladder cancer and mitigate adverse effects associated with radiotherapy. As shown in Scheme 1, after the CPC NPs accumulated in the tumor region and entered the tumor cells, H_2O_2 was decomposed into toxic OH, which could induce cell death. Copper ions also took part in a reaction with intracellular GSH, resulting in a reduction of its levels. Simultaneously, the CPC NPs demonstrated CAT-like activity, interacting with overexpressed H_2O_2 to generate abundant oxygen. This oxygen production served to alleviate the hypoxic TME and increased the sensitivity of tumor cells to ionizing radiation. Moreover, under RT irradiation, CPC NPs displayed remarkable radiosensitization efficacy due to the enhanced energy deposition. Following a thorough assessment of the biosafety of the synthesized CPC NPs, the efficacy of this combined treatment approach was evaluated in mice

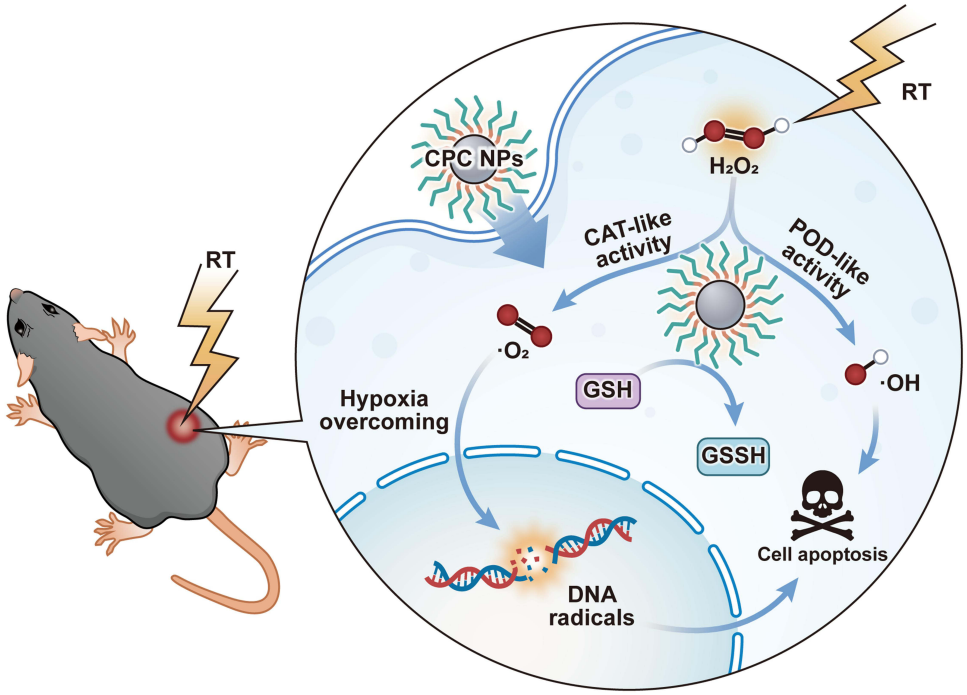

Scheme 1 Multiple functions of CPC NPs in TME under RT.

bearing subcutaneous bladder tumors. This innovative strategy introduces a novel avenue in bladder tumor therapy, demonstrating significant potential for clinical application.

Result and Discussion

Bimetallic copper and palladium (CP) NPs were synthesized using a facile method, as shown in Figure 1A and B, and demonstrated an average size of 5.3 nm (Figure S1). High resolution transmission electron microscope (HRTEM) showed an uniform lattice structure of CP NPs. The synthesized CPC NPs had a uniform spherical morphology (Figure 1C and D). Following the decoration with Cys, the zeta potential of CPC shifted from −28.8 mV to −32.3 mV (Figure 1E). Subsequently, the CP nanoparticles were demonstrated to maintain physical stability over 24 hours, with a consistent size distribution, when exposed to a cell culture medium (Figure S2). Moreover, after a 48 h observation of diameter of CP NPs, it was revealed that CP NPs showed satisfied stability in both PBS and serum (Figure S3). Further surface investigation of the surface element state of Cu and Pd in CP NPs was demonstrated in Figure 1F and G. CP NPs exhibited copper zero-valence states (Cu 2p3/2 at 932.57 eV) as well as Cu (II) 2p3/2 at 934.21 eV. Simultaneously, the high-resolution XPS spectra of palladium in Figure 1G revealed two chemical states; Pd 3d5/2 at 335.07 eV and Pd (II) 3d5/2 at 336.76 eV. The FTIR analysis of Cys, CP, and CPC NPs was also carried out. It could be inferred from Figure 1H that similar peaks of Cys appeared in the pattern of CPC, indicating successful decoration of Cys on CP NPs.

The ability of CPC to modulate the TME was assessed. Initially, the GSH-exhausting capability of the CPC NPs was evaluated in an in vitro-simulated environment with GSH. The content of GSH was measured using a GSH assay kit, as depicted in Figure 2A. No significant change in GSH levels was observed after treatment with saline, whereas a decrease in GSH levels was noted in the CPC NPs-treated groups, indicating that GSH could be continuously converted into GSSG by the CPC NPs. Subsequently, the oxygen production resulting from CPC-mediated H_2O_2 decomposition was assessed. As illustrated in Figure 2B, apparent oxygen generation was observed in the presence of CPC, indicating the CAT-like activity of CPC. Therefore, the POD-like activity was assessed using a 3,3',5,5'-Tetramethylbenzidine (TMB) kit, which underwent a color change from transparent to blue in the presence of •OH. The color of TMB turned blue upon reaction with •OH. The UV-vis spectra of oxidized TMB after CPC treatment further confirmed the POD-like activity of

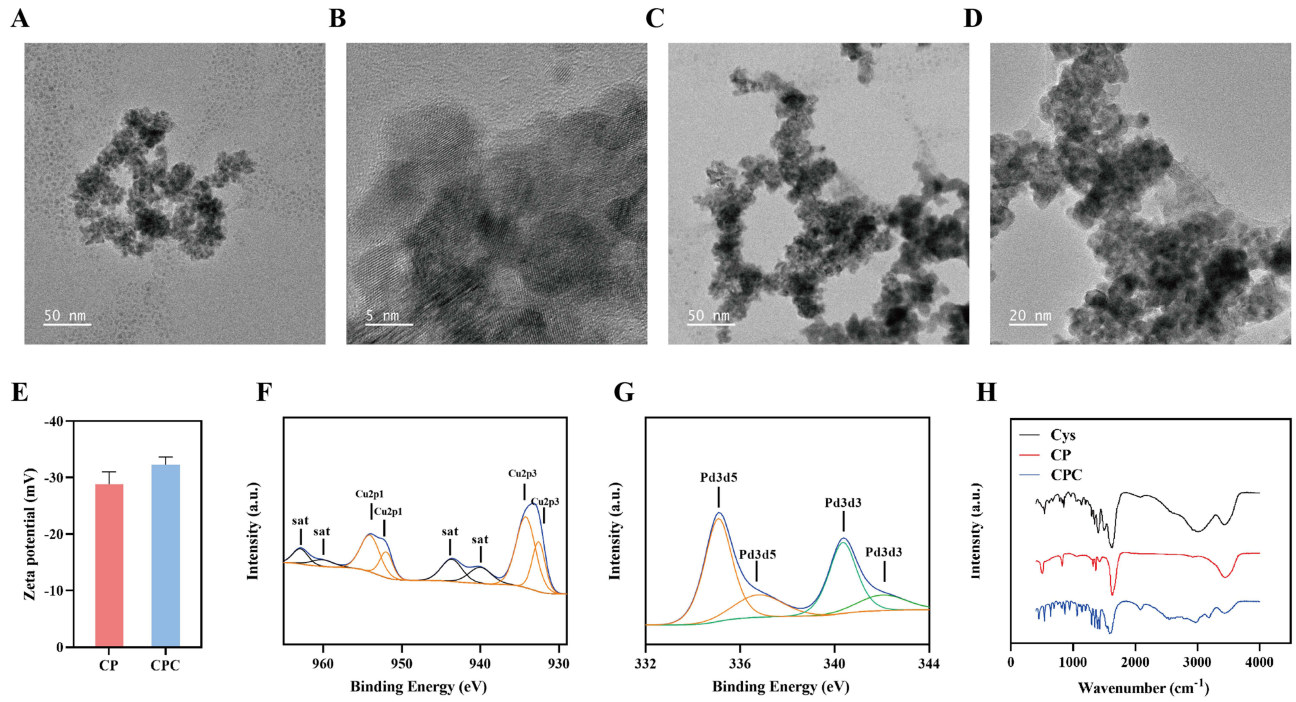

Figure 1 Characterization. (**A**) TEM images and (**B**) HRTEM images of CP. (**C**) TEM images and (**D**) HRTEM images of CPC NPs. (**E**) Zeta potential of CP and CPC NPs. High-resolution XPS spectra of (**F**) Cu orbit and (**G**) Pd orbit. (**H**) FTIR spectra of Cys, CP, and CPC NPs.

CPC (Figure 2C). In Figure 2D, it can be inferred that the generation of ROS by CPC from H_2O_2 occurred by OPD kit. These results confirm the GSH consumption ability, CAT-like activity, and POD-like activity of CPC.

A CCK-8 assay was then employed to investigate the impact of the CPC NPs on RAW264.7 cell survival. As depicted in Figure S4, the majority of cells survived after treatment with CPC NPs at a concentration of 100 μg/mL, reaching a survival rate of over 80%. This result verified the remarkable biocompatibility of CPC NPs. Next, the extent of hypoxia alleviation was assessed on MB49 after PBS or CPC treatments in a hypoxia atmosphere. As shown in Figure 3A, green fluorescence intensity was obvious in the control group, indicating severe hypoxia. In comparison, green fluorescence intensity in MB49 cells was almost eliminated upon co-incubation with CPC. The western blot (WB) results in Figure 3B are consistent with the immunofluorescence confocal laser scanning micrographs (CLSM) images, which indicates the hypoxia alleviation by CPC NPs. Moreover, the hypoxia alleviation was confirmed in 5637 bladder carcinoma cells. As shown in Figure S5, green fluorescence was weaker after co-incubation with CPC NPs. Up-regulation of HIF-1α was observed in the CPC NPs treatment group (Figure S6). From these results, it can be inferred that CPC could generate abundant O_2 in vitro, which controls hypoxic status and might contribute towards alleviating radio-resistance. Next, cell viability in both normoxia and hypoxia status under treatment of various concentrations of CPC NPs was measured as depicted in Figure 3C and D. The cell cytotoxicity showed a concentration dependent manner on both 5637 and MB49 cells. Surprisingly, there is no significant difference in cell viability between groups in normoxia or hypoxia due to the CAT-mimicking property of CPC NPs which convert H_2O_2 to O_2. To further confirm intracellular efficacy, we determined the fluorescence intensity of reactive oxygen species (ROS) in vitro. CLSM (Figure 3E) show ROS generated in cells (DCFH-DA green label). In normoxia status, following a 4-hour treatment with CPC NPs, the levels of ROS in MB49 cells increased significantly, indicating the successful generation of ROS by the POD-like CPC NPs in the treated cells. Moreover, the fluorescence intensity in the cells was further increased when combined with RT irradiation. In comparison, the green fluorescence reduced in cells treated with RT only in a hypoxia status compared with normoxia status, indicating radio-resistance resulted from hypoxia. However, when applied with CPC NPs before RT, significant amount of ROS generation was observed. The POD-like and CAT-like property of CPC NPs attributed to the ROS generation both directly and indirectly by modulation of TME to enhance radio-sensitivity. Subsequently, since radiotherapy induces

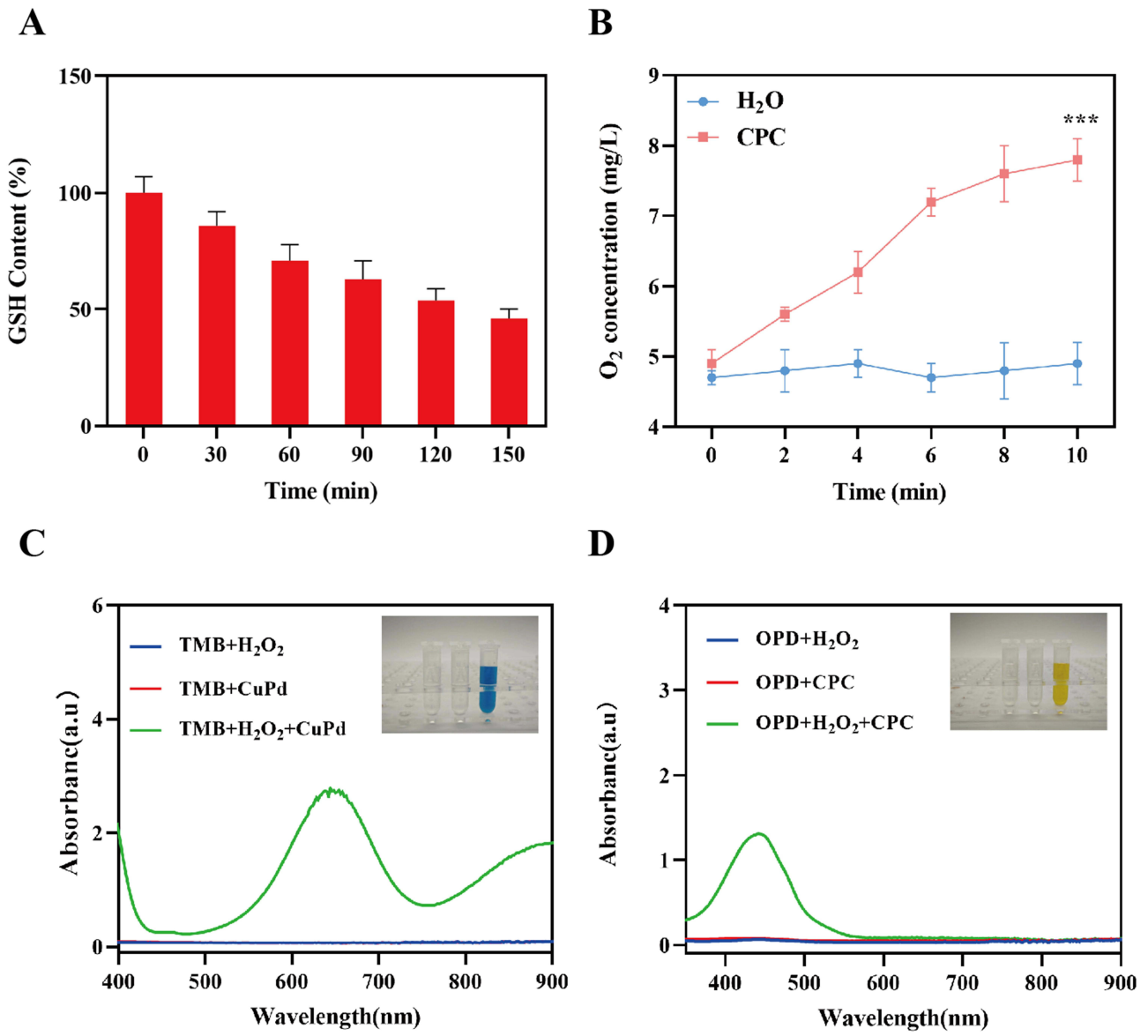

Figure 2 Enzyme mimicking properties. (**A**) GSH consumption. (**B**) O_2 generation by PBS or CPC. POD-like properties assessment by UV-vis absorption spectra of (**C**) ox-TMB o and (**D**) x-OPD. Statistical significance was determined using one-way analysis of variance (ANOVA): ***p < 0.001.

cell apoptosis through direct or indirect DNA damage, the level of DNA damage was assessed using γ-H_2AX staining, and the results are demonstrated in Figure 3F. After ionizing irradiation, a slight red fluorescence intensity was observed in the RT-only group, suggesting mild DNA damage from RT. By comparison, the most severe DNA damage was observed in the CPC+RT group, indicating that CPC could efficiently enhance the DNA damage effect of RT. Next, cell apoptosis relative proteins in various treatment groups were analyzed by WB. As shown in Figure 3G, a significant increase in cleaved caspase-3 levels was observed in MB49 cells treated with CPC+RT. Meanwhile, a slight decrease in Bcl2 was evident in the RT and CPC groups, while a more apparent upregulation of Bcl2 was observed in the CPC+RT group suggesting severe cell apoptosis. Then cell viability of various treatment groups was assessed using CCK8 kit (Figure 3H). It could be inferred that RT only has a slight influence on cell viability because most of the cells survived in the group treated with RT. However, the survival rate of MB49 cells decreased when co-incubated with CPC NPs due to POD-like activity. Severe cell death was observed in the CPC + RT group compared to RT only. The experiment conducted on 5637 cells were consistent with these results (Figure S7). These results indicate that CPC NPs can enhance treatment effect of RT, achieving an excellent antitumor effect. A more pronounced cell death rate was confirmed by the

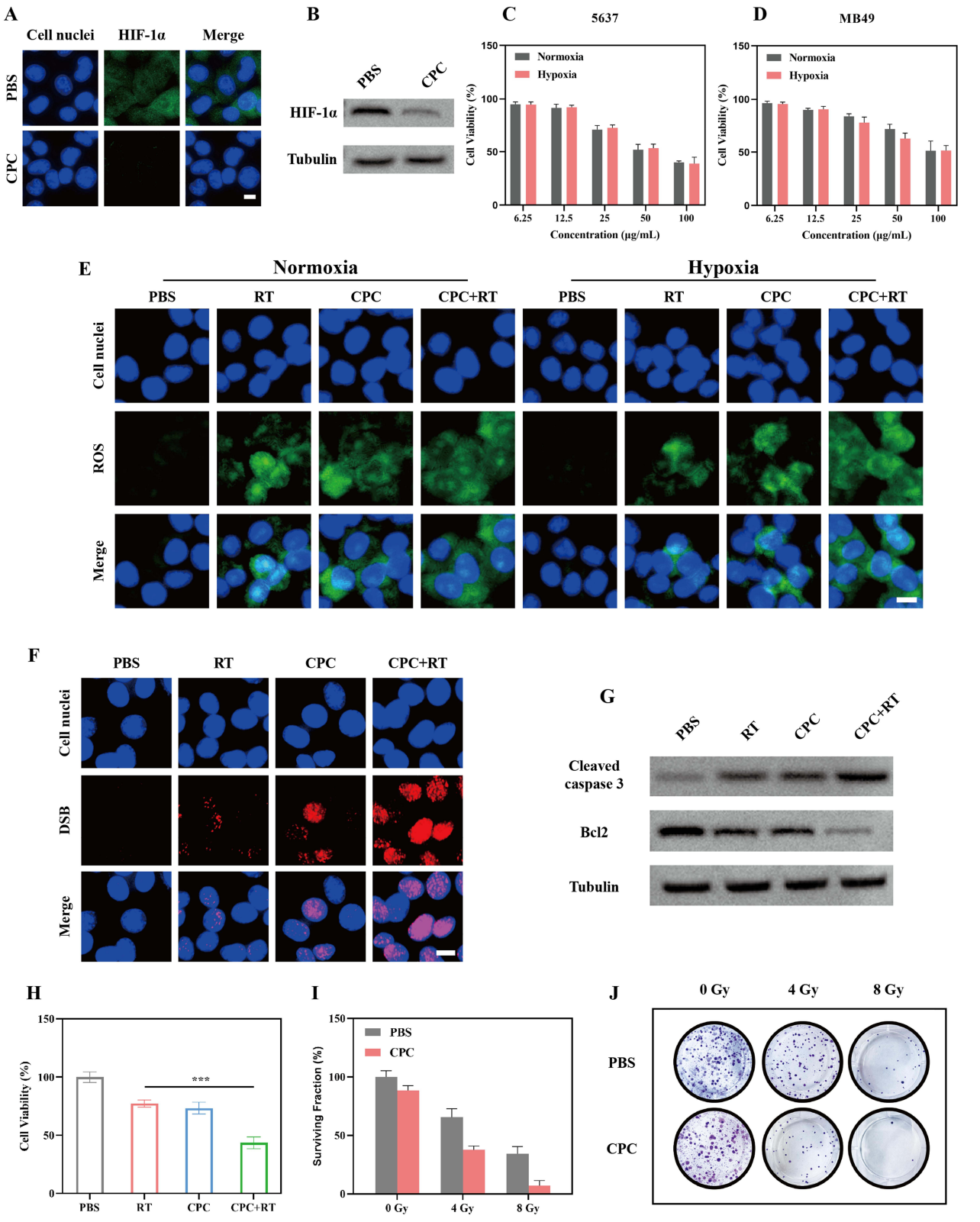

Figure 3 In vitro radiosensitization efficacy of CPC NPs. (**A**). HIF-1α immunofluorescence staining of MB49 cells treated with PBS or CPC NPs under hypoxia conditions (Scale bar: 10 μm). (**B**) WB analysis of HIF-1α protein. Cytotoxicity assay was performed on (**C**) 5637 and (**D**) MB49 cells. (**E**) ROS staining of MB49 cells under various treatments (Scale bar: 20 μm). (**F**) DNA damage assessed by γ-H_2AX staining (Scale bar: 20 μm). (**G**) Cell apoptosis-related protein analysis by WB. (**H**) Cell viability of MB49 under various treatments. (**I**) Surviving fraction and (**J**) representative images of colony formation. Statistical significance was determined using one-way analysis of variance (ANOVA): ***$p < 0.001$.

combination of CPC+RT. The evaluation of cell proliferation was thereby assessed using a colony formation assay. As illustrated in Figure 3I, the addition of CPC resulted in a significant decrease in the surviving fraction at a dosage of 8 Gy, consistent with the findings presented in Figure 3J. These results substantiate the earlier hypothesis that CPC can synergistically enhance RT.

Before the in vivo application of CPC NPs, the biosafety was first evaluated. To further evaluate the biosafety of CPC NPs, saline, and the CPC NP solution were injected intravenously into healthy mice, and the main organs and blood samples were obtained for the analysis of various indicators. Figure 4A shows that the heart, liver, spleen, lung, and kidney indices of the mice were normal following treatment and the injection of CPC NPs did not result in systemic toxicity or systemic damage in the mice. The blood analysis index in Figure 4B also proved the biosafety of CPC NPs. The results from our in vivo experiments show that the nanozyme CPC was nontoxicity.

Inspired by the outstanding in vitro efficacy along with biosafety in vivo, the anti-tumor efficacy of CPC NPs was assessed in an in vivo setting. Initially, the hypoxia modulation in vivo was assessed.Following the administration of either PBS as a control or CPC in mice bearing MB49 tumors, the mice were sacrificed after 24 hours, and the tumors were collected for HIF-1α staining. The green fluorescence indicative of HIF-1α signals in Figure 5A displayed a downregulation after the administration of CPC compared to PBS. Hereby, the result suggests that CPC NPs could efficiently alleviate hypoxia status,

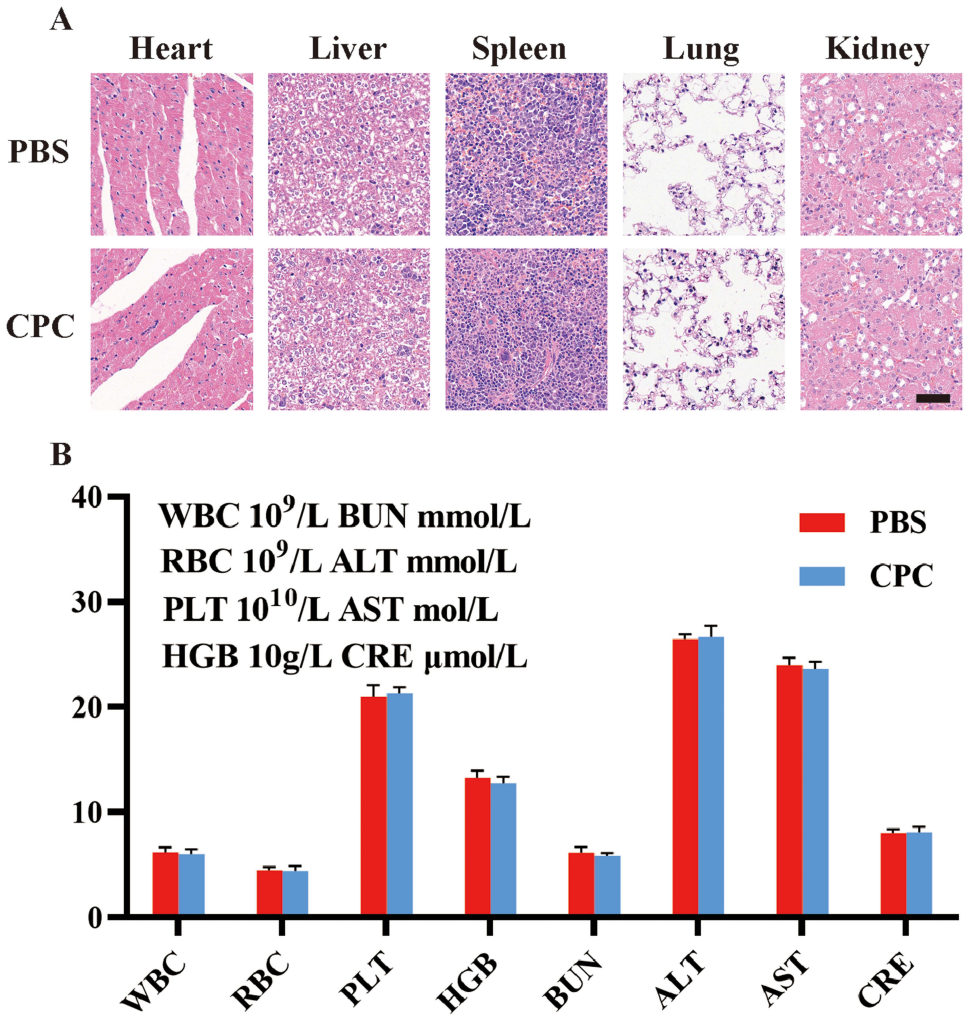

Figure 4 Biosafety evaluation. (**A**) HE staining of main organs (Scale bar: 50 μm). (**B**) Blood index analysis. Before the in vivo application of CPC NPs, the biosafety was first evaluated. To further evaluate the biosafety of CPC NPs, saline, and the CPC NP solution were injected intravenously into healthy mice, and the main organs and blood samples were obtained for the analysis of various indicators. (**A**) shows that the heart, liver, spleen, lung, and kidney indices of the mice were normal following treatment and the injection of CPC NPs did not result in systemic toxicity or systemic damage in the mice. The blood analysis index in (**B**) also proved the biosafety of CPC NPs. The results from our in vivo experiments show that the nanozyme CPC was nontoxicity.

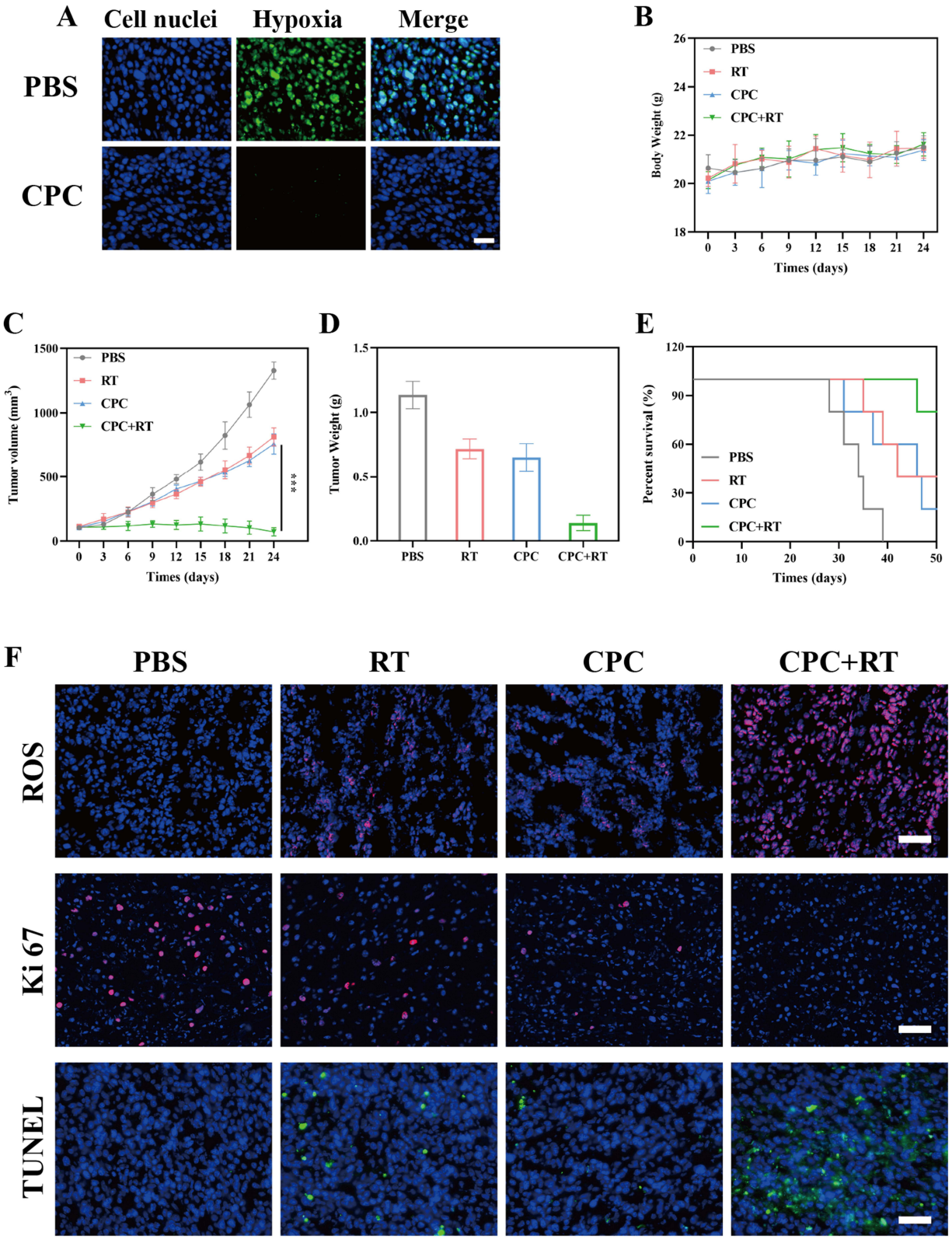

Figure 5 Radiosensitization in vivo. (**A**) Representative hypoxia staining of MB49 tumor-bearing mice after administration of PBS or CPC NPs (Scale bar: 50 μm). (**B**) Body weight, (**C**) tumor volume, (**D**) tumor weight, and (**E**) survival curve of mice under various treatments. (**F**) ROS, Ki67, and TUNEL staining of tumors from mice in different treatment groups (Scale bar: 50 μm). Statistical significance was determined using one-way analysis of variance (ANOVA): ***p < 0.001.

which might be attributed to enhancing the therapeutic efficacy of RT. Subsequently, twenty MB-49 tumor-bearing mice were randomly divided into four groups. When the tumor volume reached 100 mm^3, two groups of 10 mice each were intravenously injected with various treatments. In the first group, normal saline was administered, with 5 mice undergoing RT irradiation and the other 5 serving as the control group. In the second group, CPC NPs in PBS were intravenously injected, and among these, the tumor sites of 5 mice were subjected to RT irradiation. The body weights (Figure 5B) and tumor volumes (Figure 5C) of the mice were recorded every 3 days. Throughout the 24-day observation period, the stability of the mice's body weights was noted, indicating negligible systemic toxicity of the CPC NPs. As shown in Figure 5C, the tumor growth was rapid and completely uncontrolled in the saline group. Meanwhile, the group of mice subjected to RT alone showed an apparent tumor inhibition but the tumor growth was not under control, indicating that RT alone could not prevent tumor rapid growth. The tumor volume increased rapidly in the group treated with RT only, suggesting that no obvious therapeutic effect was induced under RT. It was evident that CPC showed a slight inhibition of tumor growth with a rate of 42.9%, attributed to the nanozyme-like properties of CPC NPs (Table S1). In contrast to the RT group, mice subjected to CPC + RT displayed outstanding tumor suppression at precisely 94.5%. These findings underscore a robust synergistic effect of NPs in conjunction with RT. The tumor weight in different treatment groups, as illustrated in Figure 5D, aligns with the findings in the tumor volume change curve. Notably, CPC+RT exhibited an extended survival time compared to other groups, achieving an impressive 80% survival rate at day 50 (Figure 5E). Representative images of immunofluorescence staining of tumors harvested in various treatments are presented in Figure 5F. DHE staining of the tumors in the four groups was conducted to assess ROS generation. As anticipated, the groups treated with PBS displayed no apparent red fluorescence, indicating minimal ROS production. Tumors in groups that received CPC administration or RT alone showed increased levels of ROS generation. Notably, the CPC + RT group displayed the highest fluorescence intensity, possibly attributed to the inability to scavenge ROS effectively. Subsequently, the POD-like reaction generated a substantial amount of ROS. The addition of RT further amplified ROS generation mediated by CPC NPs, exacerbating damage and resulting in a surge in ROS levels and GSH consumption of CPC NPs which inhibit ROS clearance. Ki67 staining, indicative of cell proliferation, was subsequently conducted. It can be inferred that red fluorescence representing Ki67 was nearly eliminated under CPC+RT treatment, signifying the effective suppression of cancer cell proliferation following this combined treatment. TUNEL staining confirmed the most pronounced cell apoptosis in the CPC+RT group. This process validates the potential of "three in one" nanozyme CPC for radio-sensitization, offering a promising approach for the treatment of bladder cancer.

Conclusion

In conclusion, ultrasmall CPC NPs were fabricated through a straightforward method, presenting a promising avenue for the synergistic therapy of bladder tumors. These NPs efficiently consumed intracellular GSH and overexpressed H_2O_2, generating toxic ROS through POD-like activity while concurrently alleviating hypoxia in the TME by producing abundant oxygen. This triple action led to induced tumor cell death and blocking of tumor cell self-repair mechanisms due to GSH depletion. Additionally, the CPC NPs demonstrated notable radiosensitization ability by modulating TME and promoting energy decomposition. The combination of CPC with RT significantly increased ROS production, enhancing RT efficacy. Interestingly, CPC NPs displayed no apparent systemic toxicity, ensuring safe usage, and achieved an impressive tumor inhibition rate of 94.5% in RT combination therapy. The simplicity of synthesis, biosafety, and exceptional therapeutic outcomes highlight the potential of CPC+RT as an outstanding candidate for bladder tumor treatment.

Acknowledgments

This work is supported by Natural Science Foundation of China (Grant No. 82202312). Please refer to Supplementary Experimental Section 1 for experimental procedure.

Author Contributions

All authors made a significant contribution to the work reported, whether that is in the conception, study design, execution, acquisition of data, analysis and interpretation, or in all these areas; took part in drafting, revising or critically reviewing the article; gave final approval of the version to be published; have agreed on the journal to which the article has been submitted; and agree to be accountable for all aspects of the work.

Disclosure

The authors report no conflicts of interest in this work.

References

1. Kaufman DS, Shipley WU, Feldman AS. Bladder cancer. *Lancet*. 2009;374(9685):239–249. doi:10.1016/S0140-6736(09)60491-8
2. Sanli O, Dobruch J, Knowles MA, et al. Bladder cancer. *Nat Rev Dis Primers*. 2017;3(1):17022. doi:10.1038/nrdp.2017.22
3. Matulewicz RS, Sharma V, McGuire BB, Oberlin DT, Perry KT, Nadler RB. The effect of surgical duration of transurethral resection of bladder tumors on postoperative complications: an analysis of ACS NSQIP data. *Urol Oncol*. 2015;33(8):338.e319–338.e324. doi:10.1016/j.urolonc.2015.05.011
4. Danna BJ, Metcalfe MJ, Wood EL, Shah JB. Assessing symptom burden in bladder cancer: an overview of bladder cancer specific health-related quality of life instruments. *Bladder Cancer*. 2016;2(3):329–340. doi:10.3233/BLC-160057
5. Grasso M. Bladder cancer: a major public health issue. *Eur Urol Suppl*. 2008;7(7):510–515. doi:10.1016/j.eursup.2008.04.001
6. Perlis N, Krahn murray D, Boehme Kirstin E, et al. The bladder utility symptom scale: a novel patient reported outcome instrument for bladder cancer. *J Urol*. 2018;200(2):283–291. doi:10.1016/j.juro.2018.03.006
7. Sternberg CN, Donat SM, Bellmunt J, et al. Chemotherapy for bladder cancer: treatment guidelines for neoadjuvant chemotherapy, bladder preservation, adjuvant chemotherapy, and metastatic cancer. *Urology*. 2007;69(1):62–79. doi:10.1016/j.urology.2006.10.041
8. Vale C. Neoadjuvant chemotherapy in invasive bladder cancer: a systematic review and meta-analysis. *Lancet*. 2003;361(9373):1927–1934. doi:10.1016/S0140-6736(03)13580-5
9. Meeks JJ, Bellmunt J, Bochner BH, et al. A systematic review of neoadjuvant and adjuvant chemotherapy for muscle-invasive bladder cancer. *Europ urol*. 2012;62(3):523–533. doi:10.1016/j.eururo.2012.05.048
10. Galsky MD, Stensland KD, Moshier E, et al. Effectiveness of adjuvant chemotherapy for locally advanced bladder cancer. *J Clin Oncol*. 2016;34(8):825–832. doi:10.1200/JCO.2015.64.1076
11. Rosenberg Jonathan E, Carroll Peter R, Small Eric J. Update on chemotherapy for advanced bladder cancer. *J Urol*. 2005;174(1):14–20. doi:10.1097/01.ju.0000162039.38023.5f
12. Chamie K, Litwin MS, Bassett JC, et al. Recurrence of high-risk bladder cancer: a population-based analysis. *Cancer*. 2013;119(17):3219–3227. doi:10.1002/cncr.28147
13. Barani M, Hosseinikhah SM, Rahdar A, et al. Nanotechnology in bladder cancer: diagnosis and treatment. *Cancers*. 2021;13(9):2214. doi:10.3390/cancers13092214
14. Silina L, Maksut F, Bernard-Pierrot I, et al. Review of experimental studies to improve radiotherapy response in bladder cancer: comments and perspectives. *Cancers*. 2021;13(1):87.
15. Wang M, Chang M, Li C, et al. Tumor-microenvironment-activated reactive oxygen species amplifier for enzymatic cascade cancer starvation/chemodynamic /immunotherapy. *Adv Mater*. 2022;34(4):2106010. doi:10.1002/adma.202106010
16. Tian Q, Xue F, Wang Y, et al. Recent advances in enhanced chemodynamic therapy strategies. *Nano Today*. 2021;39:101162. doi:10.1016/j.nantod.2021.101162
17. Meng X, Zhang X, Liu M, Cai B, He N, Wang Z. Fenton reaction-based nanomedicine in cancer chemodynamic and synergistic therapy. *Appl Mater Today*. 2020;21:100864. doi:10.1016/j.apmt.2020.100864
18. Nicholas NS, Apollonio B, Ramsay AG. Tumor microenvironment (TME)-driven immune suppression in B cell malignancy. *Biochim Biophys Acta Mol Cell Res*. 2016;1863(3):471–482. doi:10.1016/j.bbamcr.2015.11.003
19. Jing X, Yang F, Shao C, et al. Role of hypoxia in cancer therapy by regulating the tumor microenvironment. *Mol Cancer*. 2019;18(1):157. doi:10.1186/s12943-019-1089-9
20. Suo M, Liu Z, Tang W, et al. Development of a novel oxidative stress-amplifying nanocomposite capable of supplying intratumoral H2O2 and O2 for enhanced chemodynamic therapy and radiotherapy in patient-derived xenograft (PDX) models. *Nanoscale*. 2020;12(45):23259–23265. doi:10.1039/D0NR06594C
21. Lin H, Chen Y, Shi J. Nanoparticle-triggered in situ catalytic chemical reactions for tumour-specific therapy. *Chem Soc Rev*. 2018;47(6):1938–1958. doi:10.1039/C7CS00471K
22. Lu X, Gao S, Lin H, et al. bioinspired copper single-atom catalysts for tumor parallel catalytic therapy. *Adv Mater*. 2020;32(36):2002246. doi:10.1002/adma.202002246
23. Fang C, Deng Z, Cao G, et al. Co–ferrocene mof/glucose oxidase as cascade nanozyme for effective tumor therapy. *Adv Funct Mater*. 2020;30(16):1910085. doi:10.1002/adfm.201910085
24. Fan K, Xi J, Fan L, et al. In vivo guiding nitrogen-doped carbon nanozyme for tumor catalytic therapy. *Nat Commun*. 2018;9(1):1440. doi:10.1038/s41467-018-03903-8
25. Xu B, Cui Y, Wang W, et al. Immunomodulation-enhanced nanozyme-based tumor catalytic therapy. *Adv Mater*. 2020;32(33):2003563. doi:10.1002/adma.202003563
26. Liu J, Dong S, Gai S, et al. Design and mechanism insight of monodispersed aucupt alloy nanozyme with antitumor activity. *ACS Nano*. 2023;17(20):20402–20423. doi:10.1021/acsnano.3c06833
27. García S, Zhang L, Piburn GW, Henkelman G, Humphrey SM. Microwave synthesis of classically immiscible rhodium–silver and rhodium–gold alloy nanoparticles: highly active hydrogenation catalysts. *ACS Nano*. 2014;8(11):11512–11521. doi:10.1021/nn504746u
28. Cheng Y, Xia Y-D, Sun Y-Q, Wang Y, Yin X-B. "Three-in-one" nanozyme composite for augmented cascade catalytic tumor therapy. *Adv Mater*. 2023;362308033.
29. Wang L, Zhang X, You Z, et al. A molybdenum disulfide nanozyme with charge-enhanced activity for ultrasound-mediated cascade-catalytic tumor ferroptosis. *Angew Chem Int Ed*. 2023;62(11):e202217448. doi:10.1002/anie.202217448
30. Chen T, Zeng W, Liu Y, et al. Cu-doped polypyrrole with multi-catalytic activities for sono-enhanced nanocatalytic tumor therapy. *Small*. 2022;18(29):2202964. doi:10.1002/smll.202202964
31. Saeed M, Ren W, Wu A. Therapeutic applications of iron oxide based nanoparticles in cancer: basic concepts and recent advances. *Biomater Sci*. 2018;6(4):708–725. doi:10.1039/C7BM00999B

32. Ji M, Xu M, Zhang W, et al. Structurally well-defined Au@Cu_2−xs core–shell nanocrystals for improved cancer treatment based on enhanced photothermal efficiency. *Adv Mater*. 2016;28(16):3094–3101. doi:10.1002/adma.201503201
33. Li R, Zhao W, Han Z, et al. Self-cascade nanozyme reactor as a cuproptosis inducer synergistic inhibition of cellular respiration boosting radioimmunotherapy. *Small*. 2024;20(25):2306263. doi:10.1002/smll.202306263
34. Meng X, Jia K, Sun K, Zhang L, Wang Z. Smart responsive nanoplatform via in situ forming disulfiram-copper ion chelation complex for cancer combination chemotherapy. *Chem Eng J*. 2021;415:128947. doi:10.1016/j.cej.2021.128947
35. Zhang M, Qin X, Xu W, et al. Engineering of a dual-modal phototherapeutic nanoplatform for single NIR laser-triggered tumor therapy. *J Colloid Interface Sci*. 2021;594:493–501. doi:10.1016/j.jcis.2021.03.050
36. Shrestha S, Wu J, Sah B, et al. X-ray induced photodynamic therapy with copper-cysteamine nanoparticles in mice tumors. *Proc Natl Acad Sci*. 2019;116(34):16823–16828. doi:10.1073/pnas.1900502116
37. Zhu D, Ling R, Chen H, et al. Biomimetic copper single-atom nanozyme system for self-enhanced nanocatalytic tumor therapy. *Nano Res*. 2022;15(8):7320–7328. doi:10.1007/s12274-022-4359-6
38. Feng F, Zhang X, Mu B, et al. Attapulgite doped with fe and cu nanooxides as peroxidase nanozymes for antibacterial coatings. *ACS Appl Nano Mater*. 2022;5(11):16720–16730. doi:10.1021/acsanm.2c03721
39. Ruan H, Zhang S, Wang H, et al. Single-atom Pd/CeO_2 nanostructures for mimicking multienzyme activities. *ACS Appl Nano Mater*. 2022;5(5):6564–6574. doi:10.1021/acsanm.2c00644
40. Chen X, Jia Z, Wen Y, et al. Bidirectional anisotropic palladium nanozymes reprogram macrophages to enhance collaborative chemodynamic therapy of colorectal cancer. *Acta Biomater*. 2022;151:537–548. doi:10.1016/j.actbio.2022.08.020